OPTIMIZATION OF ZIGZAG PRINTED CIRCUIT HEAT EXCHANGER STRUCTURE FOR PARTICLE DEPOSITION BASED ON DEPOSITION MODEL

Ying Xu[1,2,3], Yu-Shuang Chen[1,2,3], Xiao-Hong Yang[1], Yang Zou [1,2,3*]*

[1]*Shanghai Institute of Applied Physics, Chinese Academy of Sciences, 201800, Shanghai, China*
[2]*National Key Laboratory of Thorium Energy, Shanghai Institute of Applied Physics, Chinese Academy of Sciences, 201800, Shanghai, China*
[3]*University of Chinese Academy of Sciences, 100049, Beijing, China*
**zouyang@sinap.ac.cn, chenyushuang@sinap.ac.cn.*

Keywords: MICRO-CHANNEL EXCHANGER, PARTICLE DEPOSITION, DISCRETE PARTICLE MODEL(DPM), NUMERICAL SIMULATION

Abstract

The micro-channel heat exchanger represents a pivotal component within the molten salt reactor system, responsible for heat transfer operations. The deposition behaviour of impurity within this apparatus has the potential to compromise the efficiency of heat transfer, thereby impacting the long-term operational stability of the whole system. In this study, we conducted a systematic investigation of the deposition characteristics of impurity particles in micro-channel heat exchangers using numerical simulations based on the critical velocity model. The orthogonal design method was employed to analyze the effects of zigzag structural parameters, inlet velocity, and inlet temperature on particle deposition characteristics. The results indicate that within the examined parameters ranges, the optimal combination of channel parameters for minimizing particle deposition rate is a channel diameter of 4 mm, a zigzag angle of 15° , and a pitch length of 10 mm. The influence of various factors on particle deposition rate is ranked as follows: channel diameter > inlet velocity > zigzag angle > pitch length > inlet temperature. The findings of this study provide important theoretical insights into the understanding of particle deposition behavior in micro-channel heat exchangers for MSR systems and offer valuable guidance for the optimization of heat exchanger design.

1 Introduction

Thorium-based molten salt reactor nuclear energy system (TMSR) constitutes a pivotal component of the Chinese Academy of Sciences' strategic priority research program, garnering significant attention due to its notable advantages in economic efficiency, heat transfer performance, safety, and environmental compatibility[1]. With the rapid advancement of molten salt reactor technology toward miniaturization and modularization, higher demands for compactness have been placed on molten salt heat exchangers, which are critical for thermal transport. In this context, the printed circuit heat exchanger (PCHE) has emerged as the preferred heat exchange equipment for small modular molten salt reactors, owing to its exceptional compactness, high thermal efficiency, and outstanding resistance to high temperatures and pressures. Among various PCHE configurations, the zigzag PCHE has become a focal point of research due to its simplicity in manufacturing and high feasibility.

During the operation of molten salt reactors, the corrosive and erosive effects of molten salt on graphite can generate graphite particles. Additionally, noble metal solid fission products, molten salt corrosion products, and solid oxide byproducts may be carried by the molten salt flow into the micro-channel heat exchanger. The channel diameter of zigzag PCHEs typically ranges from 0.5 mm to 4 mm. While such micro-channel dimensions significantly enhance heat transfer efficiency, they also introduce new challenges. Due to the small channel size, impurity particles may collide with and deposit on the heat exchanger walls as they traverse the micro-channels. Particle deposition gradually reduces the cross-sectional area of the internal flow channels, leading to a significant increase in system pressure drop. In severe cases, this may even cause blockages within the heat exchanger, thereby compromising the long-term stable operation of the entire reactor system. Therefore, an in-depth investigation of particle deposition behavior in micro-channel heat exchangers is of both theoretical and practical significance for elucidating the deposition mechanisms of impurity particles, optimizing heat exchanger design to reduce deposition probability, and ensuring prolonged system stability.

In recent years, numerous researchers have extensively studied particle deposition behavior based on critical particle deposition velocity models. Brach and Dunn[2] proposed a critical kinetic energy model based on the Johnson-Kendall-Roberts (JKR)[3] theory to predict the critical velocity for particle deposition and validated its accuracy for particle collisions with surfaces of different materials through experimental comparisons. Lu et al.[4] employed the Reynolds Stress Model (RSM) and Discrete Phase Model (DPM) to investigate the influence of structural shapes on particle deposition distribution in turbulent gas flows, demonstrating a strong correlation between deposition patterns and geometry. Li et al.[5] applied a critical velocity model to numerically

simulate ash particle deposition on novel inclined heat transfer surfaces, confirming the feasibility of the method through comparisons with experimental data. Liu et al.[6] utilized a critical velocity model to numerically analyze the effects of inlet velocity, temperature, channel structure, and particle size on deposition characteristics in enhanced pipes, revealing that deposition rates and fouling thermal resistance increase significantly with higher inlet velocity, temperature, bend angle, and particle size. Li et al.[7] conducted numerical simulations of particle deposition in straight pipes, finding that deposition velocity increases with particle diameter. Zhang et al.[8] investigated deposition characteristics on grooved blades using a critical velocity model, demonstrating that groove structures effectively reduce overall deposition efficiency.

Although existing studies have successfully elucidated particle deposition patterns in various channel structures based on critical deposition velocity models, research on the transport and deposition characteristics of impurity particles in molten salt within micro-channel heat exchangers remains unexplored. This study employs a critical deposition model, combined with numerical simulation and orthogonal experimental design, to systematically investigate the optimal geometric parameters (channel diameter, zigzag angle, and pitch length) of micro-channel heat exchangers in molten salt reactors to minimize particle deposition rates. The findings provide theoretical insights and practical guidance for the optimized design and long-term stable operation of micro-channel heat exchangers in molten salt reactors.

2. Methodology

2.1 Physical model description

Zigzag PCHE consists of alternating stacked hot and cold plates, each containing multiple distributed channels. Given the complexity of the full-scale model and the periodic nature of both channel distribution and flow direction, a simplified computational model was adopted in this study to improve computational efficiency. As illustrated in Fig. 1, the numerical model comprises one hot channel and one cold channel.

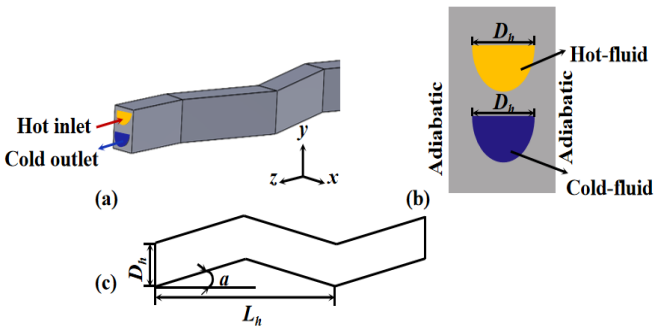

Fig. 1 The model of numerical simulation

This study primarily investigates the influence of three geometric parameters on particle deposition characteristics in zigzag PCHEs: channel diameter (D_h), zigzag angle (a), and pitch length (L_h). Through systematic analysis of particle deposition rates under different parameter combinations, the underlying mechanisms are elucidated. The specific parameter settings and investigated ranges are detailed in Table 1.

Table 1. Design parameters

Level	Channel diameter D_h / mm	Zigzag angle a/ °	Pitch length L_h/ mm
1	0.5	15	10
2	0.9	20	16
3	2	25	22
4	3	30	28
5	4	45	34

2.2 Mathematic model description

In this paper, the RNG k-ε model is adopted for turbulent flow calculations. This model features a viscosity correction term, which enhances the accuracy at low Reynolds numbers for molten salt. Additionally, it can effectively capture the turbulent structures generated by disturbances. The transport equations for turbulent kinetic energy (k) and turbulent dissipation rate (ε) are as follows:

$$\frac{\partial}{\partial xi}(\rho k u_i)=\frac{\partial}{\partial xi}(\alpha_k \mu_{eff}\frac{\partial k}{\partial xi})+G_k+G_b-\rho\varepsilon \quad (1)$$

$$\frac{\partial}{\partial xi}(\rho\varepsilon u_i)=\frac{\partial}{\partial xi}(\alpha_\varepsilon \mu_{eff}\frac{\partial \varepsilon}{\partial xi})+C_{1\varepsilon}\frac{\varepsilon}{k}(G_k+C_{3\varepsilon}G_b)-C_{2\varepsilon}\rho\frac{\varepsilon^2}{k}-R_\varepsilon \quad (2)$$

where,

$$G_k=-\rho\overline{u_i'u_j'}\frac{\partial u_i}{\partial x_i},G_b=\beta g_i\frac{\mu_t}{Pr_t}\frac{\partial T}{\partial x_i},\beta=-\frac{1}{\rho}(\frac{\partial\rho}{\partial T}),\mu_t=\rho C_\mu\frac{k^2}{\varepsilon} \quad (3)$$

$$R_\varepsilon=\frac{C_\mu\rho\eta^3(1-\eta/\eta_0)}{1+\beta_R\eta}\frac{\varepsilon^3}{k},\eta=\sqrt{2E_{ij}E_{ij}}\frac{k}{\varepsilon},E_{ij}=\frac{1}{2}(\frac{\partial u_i}{\partial x_j}+\frac{\partial u_j}{\partial x_i}) \quad (4)$$

In Eqs. (1) - (4), k is the turbulent kinetic energy, α_k、α_ε are the reciprocals of the Prandtl numbers for k and ε the effective Prandtl number, respectively. μ_{eff} denotes the effective dynamic viscosity. G_k is the turbulent kinetic energy induced by the mean velocity gradient, and G_b is the turbulent kinetic energy generated by buoyancy. ε represents the turbulent dissipation rate, and $C_{1\varepsilon}$、$C_{2\varepsilon}$、$C_{3\varepsilon}$ are empirical constants. The additional term R_ε is included in the equations to accommodate calculations for flows with rapidly changing strain rates and streamline curvatures. Where, the parameter is defined as C_μ = 0.0845, $C_{1\varepsilon}$ = 1.42, $C_{2\varepsilon}$ = 1.68, Pr_t = 0.85, β = 0.012, η_o = 4.38. $C_{3\varepsilon}$ = tanh|v_2/v_1|, where v_1 and v_2 are the velocity components parallel and perpendicular to the gravitational vector, respectively.

In Lagrangian coordinates, particle tracking is performed using the particle force equation and the Discrete Phase Model (DPM), assuming that particles exhibit neither rotation nor interaction. Conventionally, particles are typically modeled as uniform spherical entities. Nevertheless, in practical applications, particles often assume irregular shapes. Owing to the influence of shape factors, irregular particles may demonstrate higher probabilities of being captured or rebounding. Consequently, the simplifying assumption of uniform spherical particles may lead to an underestimation of the deposition rate. The equations of motion for the particles can be expressed as follow[9]:

$$m_p \frac{du_p}{dt} = \sum F_i = F_G + F_D + F_T + F_S + F_B \quad (5)$$

In Equation (5), F_G[10], F_D[11], F_T[11], F_S[12], and F_B[13] represent gravity, buoyancy, drag, thermal stroke, Saffman lift, and Brownian force, respectively. Their calculation formulas are as follows:

$$F_G = \frac{g(\rho_p - \rho)}{\rho_p} \quad (6)$$

$$F_D = \frac{1}{8}\pi C_D d_p{}^2 \rho \left|u - u_p\right| (u - u_p) \quad (7)$$

$$F_T = -D_{T,p} \frac{1}{m_p T} \frac{dT}{dx} \quad (8)$$

$$F_s = \frac{2\rho K v^{0.5} S_{ij}}{\rho_p (S_{lk} S_{kl})^{1/4}} (u_{f,j} - u_{p,j}) \quad (9)$$

$$F_B = \zeta_i \sqrt{\frac{\pi S_0}{\Delta t}} \quad (10)$$

In the above formula, g is the gravitational acceleration; ρ_p and ρ represent the particle density and fluid density, respectively; d_p is the particle diameter; u and u_p are the fluid velocity and particle velocity, respectively; C_D is the nonlinear drag coefficient; $D_{T,p}$ denotes the thermophoretic coefficient; K is a constant; $S_{i,j}$ and S_0 are the deformation sensor and Gaussian white noise random function, respectively; and ζ_i is a random integer with a typical distribution.

2.3 Particle deposition model

The deposition behavior of particles upon reaching a surface is determined by comparing their impact velocity with the critical deposition velocity. This critical velocity serves as the fundamental criterion for particle deposition — when the normal component of a particle's velocity falls below this threshold, the particle will be captured and deposited on the surface; conversely, it will rebound and be carried away by the fluid flow. The critical velocity is calculated using the following equation[2]:

$$u_{cr} = \left[\frac{2J}{d_p R^2}\right]^{10/7} \quad (11)$$

In Equation (11), R represents the coefficient of restitution, and J denotes the effective stiffness parameter, which can be expressed as:

$$J = 0.51\left[\frac{5\pi^2 (k_s + k_p)}{4\rho_p{}^{3/2}}\right] \quad (12)$$

where, $k_s = (1 - v_s{}^2)/\pi E_s$ and $k_p = (1 - v_p{}^2)/\pi E_p$, and, v_s and v_p represent the Poisson's ratios of the deposition surface and particle, respectively ($v_s = 0.31$, $v_p = 0.2$). E_s denotes the Young's modulus of the deposition surface ($E_s = 2.15\times10^{11}\ pa$), while E_p corresponds to the Young's modulus of the particle. In this study, E_p is calculated using an empirical formula for low-viscosity particles[8]:

$$E_p = 3\times10^{20} \times e^{-0.023165\times T_{avg}} \quad (13)$$

where, T_{avg} represents the average temperature of the particles and the surface.

2.4 Boundary conditions

The boundary conditions for the micro-channel adopt a velocity inlet and a pressure outlet, while the wall boundaries of the top, bottom, left, and right sides are all set as no-slip boundary conditions. The calculation is divided into two steps. First, the temperature field and flow field of the fluid are calculated, and convergence is achieved when all residuals are less than 1e-6. Then, 10,000 particles with diameters of 1μm, 5μm, 10μm, 15μm, and 20μm are respectively injected at the hot fluid inlet at the same velocity as the fluid. The positions and velocities of the particles are tracked by the DPM, and the maximum time step for the particle trajectories is 50,000. The inlet and outlet boundary conditions of the hot-side channel are both set to "escape". Using the macro DEFINE_DPM_BC in a user-defined function (UDF), we determine whether particles are deposited on the heat transfer surface. The specific calculation process is shown in Fig. 2.

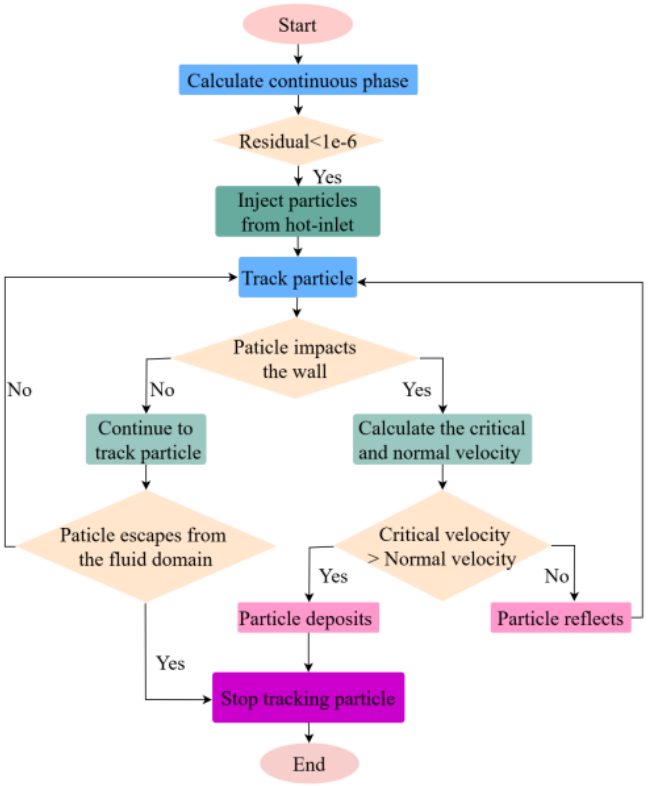

Fig. 2 Calculation flow

In this study, nuclear graphite (IG-110) was selected as the particle material. The working fluids on the hot and cold sides are FLiBe and FLiNaK, respectively, while the solid components are made of Hastelloy. The specific physical properties are presented in Table 2.

Table 2. The thermophysical properties of the deposition model

Properties	Hastelloy	IG-110[14]	FLiBe[15]	FLiNaK[16]
Density (kg/m^3)	8860	1780	2413-0.4884T	2579.3-0.624T

Specific heat (J/(kg·K))	480	710	2390	1910
Thermal conductivity (W/(m·K))	19	116	1.1	0.36+0.00056T
Viscosity (kg/(m·s))	——	——	0.116exp(3755/T)	0.024exp(4790/T)

3 Data Reduction

The calculation formula for the particle deposition rate is:

$$\eta_{dep} = \frac{N_{dep}}{N_{total}} \times 100\% \quad (14)$$

In Equation (14), η_{dep} represents the particle deposition rate, N_{dep} and N_{total} represents number of particles deposited and total injected particles.

3.1 Grid independence validation

To ensure the accuracy of calculation results, this study selects a geometric model with channel dimensions of D_h = 2 mm, a = 20°, and L_h = 10 mm for grid independence analysis. The inlet temperatures of the cold and hot sides are 803.15 K and 863.15 K, respectively, with flow velocities of 2 m/s and 1 m/s. 10,000 particles with a diameter of 10μm are injected at the inlet. Five sets of hexahedral meshes with different element numbers are generated using Fluent Meshing, and the corresponding variations in particle deposition rate are shown in Figs. 4 . The analysis results indicate that when the grid number reaches 3.99 million, the variations in particle deposition rate tend to stabilize, meeting the requirements of grid independence. Therefore, a grid division scheme with 3.99 million grids is adopted for subsequent simulation analyses, in which the boundary layer mesh is set to 8 layers, the first-layer mesh height is 0.005 mm, and the mesh growth rate near the wall is 1.2, as shown in Fig. 3.

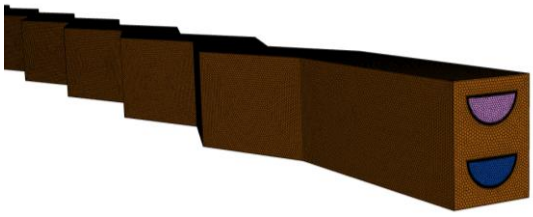

Fig. 3 Schematic diagram of model meshing

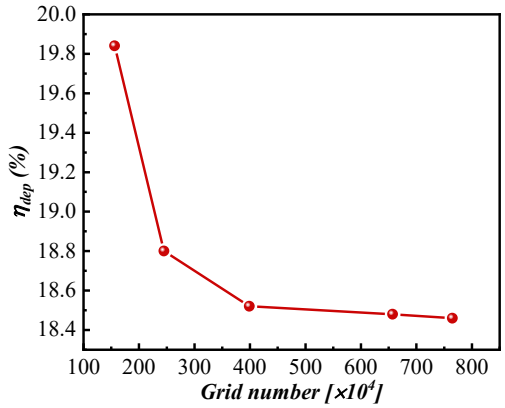

Fig. 4 Grid independent verification of calculation result

4 Orthogonal Design

To systematically investigate the influences of factors such as channel diameter (D_h), zigzag angle (a), pitch length (L_h), inlet velocity ($V_{h,in}$), and inlet temperature ($T_{h,in}$) on the particle deposition rate, this study conducted a five-level five-factor orthogonal design, as shown in Table 3.

Table 3. The orthogonal table

Case	D_h	a	L_h	$V_{h,in}$	$T_{h,in}$
A1B1C1D1E1	1(0.5mm)	1(15°)	1(10mm)	1(0.1m/s)	1(843.15K)
A1B2C3D4E5	1(0.5mm)	2(20°)	3(22mm)	4(2m/s)	5(923.15K)
A1B3C5D2E4	1(0.5mm)	3(25°)	5(34mm)	2(0.5m/s)	4(903.15K)
A1B4C2D5E3	1(0.5mm)	4(30°)	2(16mm)	5(3m/s)	3(883.15K)
A1B5C4D3E2	1(0.5mm)	5(45°)	4(28mm	3(1m/s)	2(863.15K)
A2B1C5D4E3	2(0.9mm)	1(15°)	5(34mm	4(2m/s)	3(883.15K)
A2B2C2D2E2	2(0.9mm)	2(20°)	2(16mm	2(0.5m/s	2(863.15K)
A2B3C4D5E1	2(0.9mm)	3(25°)	4(28mm	5(3m/s)	1(843.15K)
A2B4C1D3E5	2(0.9mm)	4(30°)	1(10mm	3(1m/s)	5(923.15K)
A2B5C3D1E4	2(0.9mm)	5(45°)	3(22mm	1(0.1m/s	4(903.15K)
A3B1C4D2E5	3(2mm)	1(15°)	4(28mm	2(0.5m/s	5(923.15K)
A3B2C1D5E4	3(2mm)	2(20°)	1(10mm	5(3m/s)	4(903.15K)
A3B3C3D3E3	3(2mm)	3(25°)	3(22mm	3(1m/s)	3(883.15K)
A3B4C5D1E2	3(2mm)	4(30°)	5(34mm	1(0.1m/s	2(863.15K)
A3B5C2D4E1	3(2mm)	5(45°)	2(16mm	4(2m/s)	1(843.15K)
A4B1C3D5E2	4(3mm)	1(15°)	3(22mm	5(3m/s)	2(863.15K)
A4B2C5D3E1	4(3mm)	2(20°)	5(34mm	3(1m/s)	1(843.15K)
A4B3C2D1E5	4(3mm)	3(25°)	2(16mm	1(0.1m/s	5(923.15K)
A4B4C4D4E4	4(3mm)	4(30°)	4(28mm	4(2m/s)	4(903.15K)
A4B5C1D2E3	4(3mm)	5(45°)	1(10mm	2(0.5m/s	3(883.15K)
A5B2C4D1E3	5(4mm)	1(15°)	2(16mm	3(1m/s)	4(903.15K)
A5B2C4D1E3	5(4mm)	2(20°)	4(28mm	1(0.1m/s	3(883.15K)
A5B3C1D4E2	5(4mm)	3(25°)	1(10mm	4(2m/s)	2(863.15K)
A5B4C3D2E1	5(4mm)	4(30°)	3(22mm	2(0.5m/s	1(843.15K)
A5B5C5D5E5	5(4mm)	5(45°)	5(34mm	5(3m/s)	5(923.15K)

5 Analysis of Orthogonal Results

The numerical results were analyzed using the range analysis method (as shown in Fig. 5), with the particle deposition rate as the quantitative index. M represents the mean value of the quantitative index for each factor at different levels; the higher the M value, the higher the corresponding quantitative index of the factor at that level. P is the range of the mean values of each factor, and a larger P value indicates that the factor has a more significant influence on the quantitative index.

As can be seen from Fig. 5, for the five factors of A (channel diameter), B (zigzag angle), C (pitch length), D (inlet velocity), and E (inlet temperature), their optimal levels are A5, B2, C1, D2, and E2, respectively. That is, when the channel diameter is 4 mm, the zigzag angle is 20°, the pitch length is 10 mm, the inlet velocity is 0.5 m/s, and the inlet temperature is 863.15 K, the particle deposition rate is the lowest. However, this combination is not included in the existing samples. To verify its accuracy, the combination numbered A5B2C1D2E2 was additionally calculated, and the result showed that its deposition rate was 9.99%, which was significantly higher than the minimum value of 6.06% in the existing samples. This indicates that when the range analysis method is used to analyze the particle deposition behavior in Zigzag PCHE, there is a deviation in the results. This error may be attributed to the inherent limitations of the range analysis method. The range analysis method assumes that factors are independent of each other and does not consider interactions. However, in the actual particle deposition process, significant interactions exist between factors such as channel diameter and inlet velocity, as well as zigzag angle and pitch length, which have important impacts on particle deposition behavior.

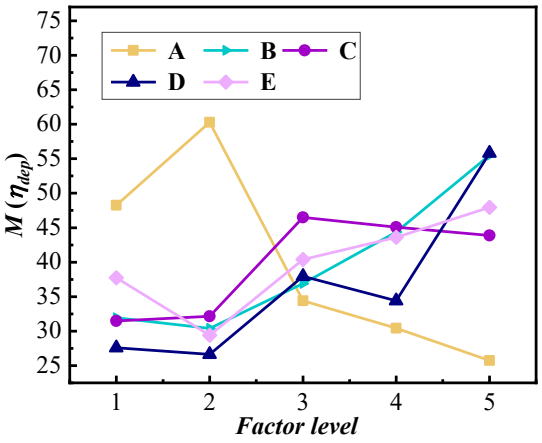

Fig. 5 The average value at different levels of different factors under method of extreme difference

The channel diameter is a key factor affecting the residence time and flow path of particles in the channel, while the inlet velocity determines the moving distance of particles per unit time. When the channel diameter is small, a lower inlet velocity significantly increases the residence time of particles in the channel, thereby increasing the possibility of particle deposition; a higher inlet velocity, conversely, causes particles to pass through the channel rapidly, reducing deposition. In contrast, for a larger channel diameter, particles require a higher inlet velocity to maintain suspension, otherwise, particles are more prone to deposition. This interaction between channel diameter and inlet velocity indicates that the influence of inlet velocity on particle deposition behavior varies significantly under different channel diameters, which is inconsistent with the results of single-factor analysis. Additionally, the zigzag angle and pitch length jointly determine the complexity of fluid flow and the turbulence intensity. A larger zigzag angle and shorter pitch length significantly increase the turbulence degree of the fluid, leading to increased particle deposition in local areas. This interaction between the zigzag angle and pitch length further indicates that under certain parameter combinations, the particle deposition behavior may deviate significantly from the prediction results considering only single factors.

Recalculation of combinations close to the predicted results and existing samples showed that the A5B1C1D1E1 combination had the lowest deposition rate, only 0.39%. Therefore, when the geometric parameters are A5B1C1 (channel diameter 4 mm, zigzag angle 15°, pitch length 10 mm), the deposition rate is the lowest.

The interaction analysis method — analysis of variance (ANOVA) was introduced to more accurately evaluate the effects of various factors and their interactions on particle deposition behavior, thereby improving the accuracy and reliability of analysis results. The significance level was used to assess the influence of each factor on the deposition rate. If the p-value was less than 0.05, the factor was considered to have a significant effect on the deposition rate. The order of influence was typically determined by the magnitude of the p-value: the smaller the p-value, the more significant the factor's impact on the deposition rate. The ANOVA results are shown in Table 4. Accordingly, the channel diameter had the greatest influence on the particle deposition rate, followed by the inlet velocity, zigzag angle, pitch length, and inlet temperature (in descending order of significance). Additionally, the inter group significance levels of channel diameter-inlet velocity and zigzag angle-pitch length were 0.03 and 0.04, respectively, indicating significant interactions between factors.

Table 4. ANOVA results

	D_h	a	L_h	$V_{h,in}$	$T_{h,in}$
p-value	0.001	0.02	0.05	0.01	0.1

6 Conclusions

This study systematically investigates the particle deposition characteristics in a zigzag channel printed circuit heat exchanger (PCHE) based on the particle rebound model and deposition model. The influences of factors such as channel diameter, zigzag angle, pitch length, inlet velocity, and inlet temperature on the particle deposition rate are evaluated using the orthogonal design method, and the optimal geometric parameter combination is determined. The main conclusions are as follows:

(1) The influence degrees of the five factors on the particle deposition rate are in the order of: channel diameter > inlet velocity > zigzag angle > pitch length > inlet temperature.

(2) The inter group significance levels of channel diameter-inlet velocity and zigzag angle-pitch length were 0.03 and 0.04, respectively, indicating significant interactions between factors.

(3) The optimal channel geometric parameters for reducing the particle deposition rate are channel diameter of 4 mm, zigzag angle of 15° , and pitch length of 10 mm.

According to the calculation results, the optimized structure of zigzag PCHE for reducing particle deposition and the deposition law of particles in the optimized structure are provided. However, this study does not consider the erosion model; thus, subsequent research will focus on simulations considering the erosion model and expand experimental studies to further deepen the verification of the particle deposition model. This finding provides an important theoretical basis for optimizing the structural design of PCHE to control particle deposition.

7 Acknowledgements

This work is supported by the “Gansu Major Scientific and Technological Special Project under Grant (Grant No.23ZDGH001) , “Youth Innovation Promotion association, Chinese Academy of Science” (Grant No.2020263), and the Thorium-based Molten Salt Reactor Nuclear Energy System Industry Fund Project (Basic Research Project) , No. SINAP-CYJJ-202401.

8 References

[1] Mianheng, J., Hongjie, X., Zhimin, D., Advanced fission energy program-TMSR nuclear energy system[J]. Bulletin of Chinese Academy of Sciences, 2012, 27(3): 366－374.

[2] Raymond M, B.，Patrick F, D. A mathematical mode of the impact and adhesion of microsphers, Aerosol Sci. Technol. 16 (1) (1992) 51－64.

[3] Kenneth Langstreth, J., Kevin, K., A. D., Roberts. Surface energy and the contact of elastic solids, in: Proceedings of the Royal Society A: Mathematical, 1971.

[4] Hao, L., Lin L. A numerical study of particle deposition in ribbed duct flow with different rib shapes[J]. Building and Environment, 2015, 94.

[5] Jinbo, Li., Wenjing, Du., Lin, C. Numerical simulation and experiment of gas-solid two phase flow and ash deposition on a novel heat transfer surface[J]. Applied Thermal Engineering, 2017, 1131033-1046.

[6] Lei, L., Ying, X., Lin, Z., et al. Numerical study of particle deposition characteristics in a new type of reinforced pipe[J]. Chemical Engineering and Processing-Process Intensification, 2023,189.

[7] Meng, L., Leren, T., Denggao, D., et al. Numerical Simulation of Particle Deposition Laws of Particulate Matter in Straight Pipes [J]. Chemical Engineering, 2023,51(07):72-77.

[8] Haosu, Z., Youxue, L., Chenlin, C., et al. Research on Particle Deposition Characteristics and Gas Film Cooling Performance of Grooved Turbine Blades [J]. Thermal Power Engineering, 2023, 38(12): 57-67.

[9] Zhimin, H., Zhiming, X., Aodi, S., Xiaoyan, Y. The deposition characteristics of micron particles in heat exchange pipelines[J]. Applied Thermal Engineering, 2019, 158113732-113732.

[10] Amy, L., Goodarz, A. Dispersion and deposition of spherical particles from point sources in a turbulent channel flow, Aerosol Sci. Tech. 16 (1992) 209－226.

[11] Putnam, A. Integrable form of droplet drag coefficient, ARS J. 31 (1961) 1467－1470.

[12] Saffman, P. G. The lift on a small sphere in a slow shear flow[J]. Journal of Fluid Mechanics, 1965, 22: 385-400.

[13] Haosu, Z., Xuelei, Y., Chenlin, C., Yuting, J. et al. Study on particle deposition characteristics and gas film cooling performance of turbine blades with grooves[J]. Journal of engineering for Thermal energy and Power, 2023,38(12):57-67.

[14] Yu, Z., Qi, W., Chunyan, Z. Neutronics and thermal-hydraulics coupled analysis on dimensional change and lifespan of graphite components in small modular molten salt reactor[J]. Nuclear Engineering and Design, 2024,425113344-.

[15] Yang Y, Yang Z, Chong Z. Conjugate heat transfer analysis of molten salt in annular heater with rectangular wire coil[J]. Results in Engineering, 2022.

[16] Yang Y., Minghai L., Yang Z., et al. Numerical study on heat transfer characteristics of molten salt in annular channel with wire coil[J]. Applied Thermal Engineering, 2021, 199.